JOURNAL OF GEOPHYSICAL RESEARCH, VOL. 107, NO. C10, 3177, doi:10.1029/2001JC001077, 2002

Breaking criteria and energy losses for three-dimensional wave breaking

Chin H. Wu
Department of Civil and Environmental Engineering, University of Wisconsin-Madison, Madison, Wisconsin, USA

H. M. Nepf
Parsons Laboratory, Department of Civil and Environmental Engineering, Massachusetts Institute of Technology, Cambridge, Massachusetts, USA

Received 31 July 2001; revised 28 March 2002; accepted 25 April 2002; published 30 October 2002.

[1] Laboratory experiments were used to explore the influence of spatial focusing and diffraction on the evolution of unsteady, three-dimensional, deep water wave packets with a constant-steepness spectrum. The wave packets were generated by 13 independently programmed paddles and evolved to breaking near the midpoint of a 4 m × 11 m test section. Detailed measurements of surface displacements were made across the entire test section and were used to examine energy losses and breaking criteria. Three forms of breaking criteria were considered: (1) geometric criteria based on local and global wave steepness, (2) a kinematic criterion based on particle and phase velocities, and (3) a dynamic criterion based on higher harmonic energy evolution. The results indicate that directionality of the waves can either increase (focusing waves) or decrease (diffracting waves) the geometric breaking criterion as well as breaking severity. In contrast, the directionality of waves had little effect on the kinematic criterion. At breaking, the ratio of local particle velocity and phase velocity was shown to be larger than unity for both focusing and diffracting waves. Indeed, the robustness and simplicity of the kinematic criterion make it an excellent choice for field application. Finally, the directionality of waves did not alter the up-frequency energy transfer associated with wave steepening. The three-dimensional, spatially focusing and diffracting wave packets lost 34% and 18% of their energy, respectively, as a result of plunging breakers and lost 12% and 9%, respectively, as a result of spilling breakers. Comparable two-dimensional breakers with the same spectral shape lost 16% for plunging and 12% for spilling. *INDEX TERMS:* 4504 Oceanography: Physical: Air/sea interactions (0312); 1255 Geodesy and Gravity: Tides—ocean (4560); *KEYWORDS:* three-dimensional breaking waves, energy dissipation, breaking criteria, directional wave

Citation: Wu, C. H., and H. M. Nepf, Breaking criteria and energy losses for three-dimensional wave breaking, *J. Geophys. Res.*, *107*(C10), 3177, doi:10.1029/2001JC001077, 2002.

1. Introduction

[2] Breaking waves are universally present over the ocean surface and play an important role in the exchange of gas, water vapor, momentum, and energy between the atmosphere and the ocean [e.g., *Kerman*, 1988; *Melville*, 1996]. These exchanges affect the growth of wind waves, the generation of sea sprays and bubbles, the formation of surface currents, and the distribution of near-surface turbulence [*Longuet-Higgins*, 1969]. The significance and study of wave breaking are excellently reviewed by *Peregrine* [1983], *Banner and Peregrine* [1993], *Thorpe* [1995], *Melville* [1996], and *Longuet-Higgins* [1997]. In view of the many important consequences of wave breaking, it is crucial to have a fundamental understanding of the breaking processes, in particular, to be able to predict the onset of breaking and its energy losses. While we have gained significant insight into the breaking process from two-dimensional laboratory experiments [*Benjamin and Feir*, 1967; *Kjeldsen and Myrhaug*, 1980; *Duncan*, 1981; *Bonmarine*, 1989; *Rapp and Melville*, 1990; *Baldock et al.*, 1996; *Kway et al.*, 1998], ultimately we must consider directionality to understand the process of breaking in the ocean, which is fully three-dimensional [*Thorpe*, 1995; *Peregrine*, 1998]. The primary purpose of this paper is to explore the effects of wave directionality (spatial focusing and diffraction) on three-dimensional breaking wave criteria and energy losses. Through comparison to other studies, the effects of spectral shape are also discussed.

[3] Many criteria have been proposed to predict the onset of wave breaking. Generally, they can be classified into three categories: (1) geometric criteria based on local wave shape [*Kjeldsen and Myrhaug*, 1980] and global wave steepness [*Rapp and Melville*, 1990]; (2) kinematic criteria based on particle and phase velocities [*Longuet-Higgins*, 1969]; and

0148-0227/02/2001JC001077$09.00

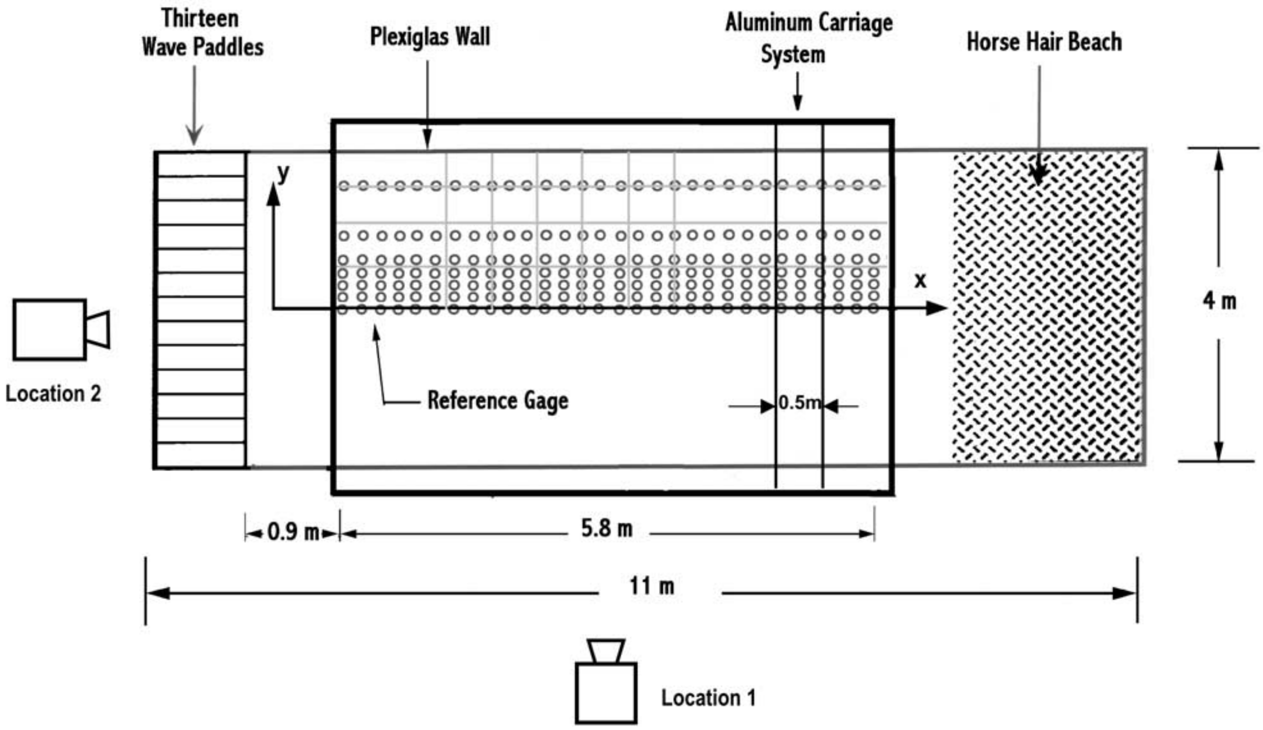

Figure 1. Top view of the test section. Circles indicate the locations of the surface displacement measurement. To verify the repeatability of waves for different runs, a reference wave gauge was kept at ($x = 120$, $y = 0$) cm. The CCD camera was positioned at location 1 (side view) and location 2 (back view). The hatched lines correspond to the position of the reference grid constructed from 1 cm ropes.

(3) dynamic criteria based on acceleration at the crest [*Longuet-Higgins*, 1969], momentum and energy growth rate [*Banner and Tian*, 1998], and higher harmonic energy evolution [*Rapp and Melville*, 1990; *Kway et al.*, 1998]. A detailed review of these breaking criteria is given by *Tulin and Li* [1992], *Easson* [1997], and *Nepf et al.* [1998].

[4] A handful of laboratory experiments have already pointed to the influence of wave dimensionality on the evolution and onset of breaking. Through instability two-dimensional wave crests with initial wave steepness greater than $ak = 0.31$ (where a is wave amplitude, k is wave number) have been shown to evolve into three-dimensional crests which eventually begin to spill [*Su*, 1982; *Su et al.*, 1982; *Melville*, 1982]. For steady, short-crested, monochromatic waves, *Kolaini and Tulin* [1995] suggested that three-dimensional effects can elevate the wave steepness at breaking. In addition, unsteady, short-crested breaking has also been shown to be influenced by directionality, with higher breaking steepnesses and greater breaking severity observed for spatially focusing waves [*She et al.*, 1994, 1997] than for diffracting waves [*Nepf et al.*, 1998]. In this paper, we expand on these results by assessing the sensitivity of several breaking criteria to wave directionality. We find that the geometric criteria are strongly affected by both directionality and spectral shape. In contrast, the kinematic and dynamic criteria appear insensitive to both directionality and spectral shape. Finally, the kinematic criterion is shown to be the most robust and promising criterion for field applications.

[5] The loss of wave energy due to breaking is a source of energy for turbulent mixing and air entrainment, which can enhance air-sea gas and heat transfer [*Jessup et al.*, 1997]. Most laboratory studies for energy loss are limited to two-dimensional waves, for example, quasi-steady breaking [*Duncan*, 1981, 1983] and unsteady breaking [*Rapp and Melville*, 1990] with the estimated loss of energy flux from a wave group ranging from 10% for a spilling breaker to 25% for a plunging breaker. These laboratory results have been used to estimate the energy dissipation for wave breaking in the field [*Thorpe*, 1993; *Melville*, 1994]. Recently, *Kway et al.* [1998] observed that the breaking losses increase as the spectral shape shifts toward the higher-frequency components, that is, moving from the constant-steepness spectrum (14%) to Pierson-Moskowitz spectrum (20%) and finally to the constant-amplitude spectrum (22%). This trend is consistent with the fact that most of the energy lost in breaking comes from the high-frequency end of the spectrum [*Rapp and Melville*, 1990]. In this paper, we show that wave directionality can also impact the loss of wave energy due to breaking.

2. Experimental Methods

[6] The study was conducted in a 4 m × 11 m test section (Figure 1) within the Gunther Family Three-dimensional Wave Basin at the Massachusetts Institute of Technology. The mean water depth was $d = 0.6$ m. A coordinate system was chosen with x as the longitudinal (wave propagation) direction and $x = 0$ at the mean paddle position; y as the lateral direction and $y = 0$ at the midpoint of test section; $z = 0$ at the mean water level and positive upward. The test section contained 13 hydraulically driven wave makers controlled by a central computer that can generate single frequency or

spectral waves from 0.4 Hz to 3.0 Hz. The transfer function between the wave maker and the observed surface displacement was determined using an impulse response method. The variation in transfer function due to temperature change was negligible. The wooden frame beach had a slope of 1:5 and was covered with 4 inches (10 cm) of horsehair material. The maximum beach reflection was 5% for monochromatic waves, based on the three-wave gauge method described by *Rosengaus-Moshinsky* [1987]. Extrapolating these results to the multifrequency wave packets, beach reflection was expected to contribute less than 5% error to the estimation of local wave-packet energy.

[7] The surface displacement was recorded using an array of 4-mm diameter, resistance-type wave gauges with 0.2 mm accuracy. The wave gauge signals were amplified and recorded at 200 Hz by a DAS1602 data acquisition board (Keithley Metrabyte) that was synchronized to the wave maker system by external analog triggering. Wave records of 80 s were measured at 210 grid positions using an aluminum carriage system that straddled the measurement area (6 m $\times$ 4 m). The carriage system held seven wave gauges at the lateral positions y = 0, 15, 30, 45, 60, 90, 150 cm; and was traversed longitudinally in x = 90 cm increments from x = 90 to 670 cm (Figure 1). A tighter lateral spacing was chosen near the centerline to capture the local details of the short-crested waves. Measurements between x = 0 and 90 cm were not considered because of interference from wave modes associated with the paddles [*Dean and Dalrymple*, 1984]. Allowing for symmetry across the centerline, the entire measurement area was scanned using 30 repeatable runs. Before each experimental run, several tests were made to verify symmetry and repeatability, and to calibrate the wave gauges. Details of these tests are given by *Nepf et al.* [1998].

[8] To compare the surface displacement measurements to the observed breaking locations, a CCD camera (COHU 4910) was used to acquire visual records of the breaking events from two viewing positions: (1) sideview and (2) backview, i.e., from atop the paddles. The camera was synchronized to the wave gauge data acquisition and the wave maker system. A PCI frame grabber board (Bitflow, Inc.) was used to acquire the images with 640 $\times$ 480 pixels for 20 s at 10 Hz. A reference grid was constructed from a 1 cm rope strung across the test section at x = 200, 250, 300, 350, 400, and 450 cm and y = 0, 50, 100, and 150 cm (hatched lines in Figure 1). After correcting for parallax, these images provided spatial resolution with 5 cm accuracy. Finally, the spatial extent of the white-capped breaking region was measured by enhancing the image contrast and delineating the region using edge detection.

2.1. Wave Generation

[9] A single, two-dimensional unsteady breaker can be generated using the constructive interference of dispersive wave components, a technique introduced by *Cummins* [1962] and *Davis and Zarnick* [1964] for testing ship models. *Longuet-Higgins* [1974], *Greenhow and Vinje* [1982], and *Rapp and Melville* [1990] extended this technique to generate an isolated breaker within a wave packet. The technique emulates the wave-wave interaction process that dominates unsteady breaking in the field, particularly associated with white-capping around the peak of the wind-wave spectrum [*Rapp and Melville*, 1990; *Tulin and Li*, 1992]. Indeed, previous laboratory results for two-dimensional breaking generated by this technique have been linked to field observations of energy dissipation [*Melville*, 1994]. In this study, we build on the frequency focusing technique by adding directionality, i.e., spatial focusing and diffraction, to the wave evolution producing three-dimensional, short-crested breakers. It is important to note that other mechanisms such as wave-current interaction [*Longuet-Higgins and Stewart*, 1961; *Kjeldsen and Myrhaug*, 1980], direct wind forcing [*Banner and Phillips*, 1974], intrinsic instability [*Benjamin and Feir*, 1967], and steady breakers produced by submerged objects [*Duncan*, 1981, 1983] can also affect the breaking processes in the field. However, these mechanisms are not considered here.

[10] The free surface displacement, $\eta(x,y,t)$ can be described by

$$\eta(x,y,t) = \sum_{n=1}^{N} a_n \cos\left[(k_n \cos\theta_n)x + (k_n \sin\theta_n)y - 2\pi f_n t + \phi_n\right], \tag{1}$$

where a_n, k_n, ϕ_n, and θ_n are the amplitude, wave number, phase, and propagation angle, respectively, for each of N wave components and f_n is the nth frequency component given by the linear relationship

$$(2\pi f_n)^2 = k_n\, g \tanh(k_n d), \tag{2}$$

where g and d are the gravitational constant and water depth, respectively. The surface displacement is thus described by the variables N, f_n, a_n, ϕ_n, and θ_n and d.

[11] To create a two-dimensional wave packet, the paddles were moved in unison so that the variables in (1) were the same for each paddle. Following *Rapp and Melville* [1990], the number of wave components, N, was chosen as 32, a number large enough to approximate a continuous spectrum. The 32 components, f_n, were equispaced across a bandwidth of Δf = 0.789 Hz and centered at frequency $f_c = (f_1 + f_{32})/2$ = 1.08 Hz. Each component amplitude was chosen to produce a constant wave steepness

$$a_n = \frac{G}{k_n}, \tag{3}$$

where G is the gain factor used to vary the overall intensity of the wave packet [*Loewen and Melville*, 1991]. In contrast to a constant-amplitude spectrum, i.e., a_n = constant, this condition inhibits premature breaking, because all components maintain similar scale with regard to steepness. In addition, the constant-steepness spectrum more closely approximates the wind-wave spectrum, i.e., $\propto f^{-5}$ [*Phillip*, 1958]. Finally, each phase component ϕ_n was determined using linear theory to achieve a theoretical focusing point at x_f = 330 cm (see Figure 2) and focusing time at t_f = 12 s. Applying the above constraints and setting the propagation angle, θ_n, to zero, the surface displacement required at each paddle, x_p, is then given by

$$\eta(x = x_P, t) = \sum_{n=1}^{N=32} \frac{G}{k_n} \cos\left[-k_n x_f - 2\pi f_n (t - t_f)\right]. \tag{4}$$

The time series of the input signal and the corresponding spectrum are shown in Figure 3. The input signal was

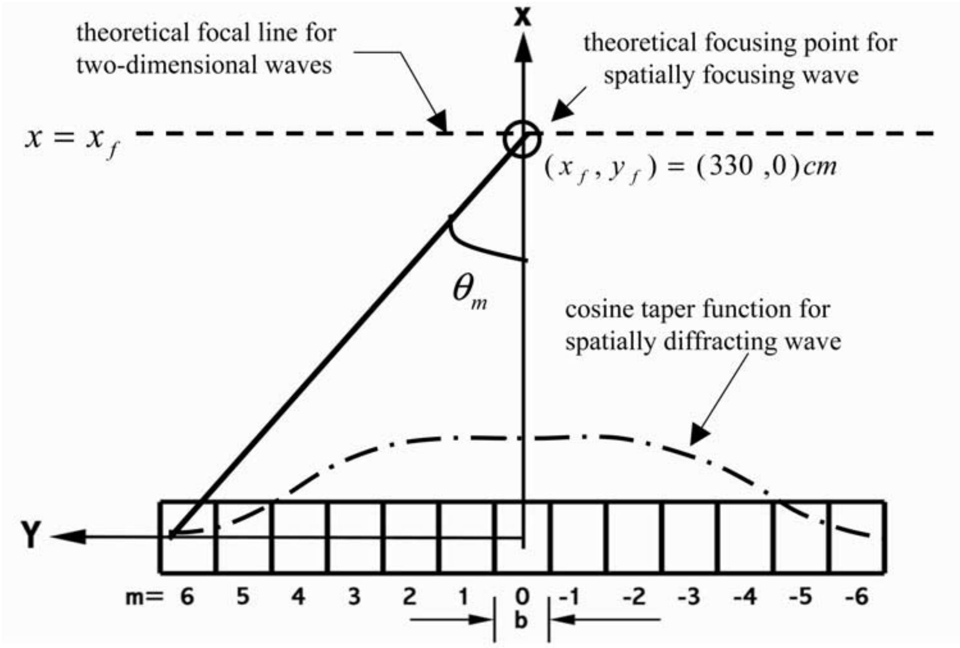

Figure 2. Schematic of 13 paddles. The dashed line is the theoretical focusing line, $x = x_f$, for the two-dimensional wave. The circle at the centerline is the theoretical focusing point, (x_f, y_f), for the three-dimensional spatially focusing wave. The dotted-dashed line is the cosine taper function for the three-dimensional spatially diffracting wave.

tapered over the first and last second to eliminate abrupt paddle movement.

[12] Using the above two-dimensional wave generation as a basis, two methods were introduced to generate short-crested waves by varying individual paddle motion. First, we consider a spatially focusing crest which may occur in the field when obliquely traveling wave packets meet, for example, after passing around an island or because of wave generation by spatially varied wind direction. To produce this wave in the laboratory, a different propagation angle θ_{mn} was selected at each paddle, m, such that the wave train from each paddle converged at position (x_f, y_f) at time $t_f = 12$ (Figure 2). The propagation angle was not varied across the frequency component, f_n, although in general it could be. The propagation angle, θ_{mn}, for the mth paddle was determined geometrically as

$$\theta_{mn} = \tan^{-1}\left(\frac{x_f}{|\,m\,|\,b}\right), \tag{5}$$

where b is the width of each paddle and m is an integer from -6 to 6. The maximum propagation angle, $\theta_{\max} = \theta_{6n}$, was used to characterize the total degree of wave focusing. The remaining parameters N, a_n, and f_n were kept the same as the two-dimensional case. To produce a frequency and spatially focusing crest, the surface displacement required at each paddle was then given by

$$\eta(x = x_P, y = mb, t) = \sum_{n=1}^{N=32} \frac{G}{k_n} \cos\Big[-k_n\big(|mb|\sin\theta_{mn} + x_f\cos\theta_{mn}\big) - 2\pi f_n\big(t - t_f\big)\Big]. \tag{6}$$

Because the paddle width and the total number of paddles were fixed by the facility, the maximum propagation angle $\theta_{\max}$ could only be varied through, x_f, the distance between the paddles and the focusing point. In this study, we considered a fixed angle, $\theta_{\max} = 31°$, prescribed by $x_f =$ 330 cm, the same focusing distance used for the two-dimensional waves. For reference, *She et al.* [1994] investigated $\theta_{\max} = 0° \sim 89°$ and found that breaking height and severity increase as $\theta_{\max}$ increases.

[13] The second type of short-crested breaking considered in this study is a diffracting wave. This wave approximates field conditions in which small-scale heterogeneity within the wind field produces small-scale heterogeneity in wave amplitude such that the wave front diffracts as it evolves to breaking through frequency focusing. To create this type of wave, a lateral variation in wave amplitude was introduced. The central paddles were moved together at the maximum amplitude and the remaining paddles were tapered down to 10% using a cosine window (Figure 2). This transverse tapering produced passive directional spreading during wave evolution. The surface displacement of the mth paddle was then described by

$$\eta(x = x_P,\, y = mb,\, t) = \begin{cases} \displaystyle\sum_{n=1}^{N=32} \frac{G}{k_n}\cos\left[-k_n x_f - 2\pi f_n\left(t - t_f\right)\right], & |m| < \frac{L_o}{2b} \\ \displaystyle\sum_{n=1}^{N=32} \frac{G}{k_n}\cos\left[-k_n x_f - 2\pi f_n\left(t - t_f\right)\right]\left[0.1 + 0.9\cos^2\left(\frac{m\pi}{12}\right)\right], & |m| > \frac{L_o}{2b}, \end{cases} \tag{7}$$

where L_o is the length of central paddles without tapering. The degree to which diffraction impacts breaking dynamics depends on both L_o as well as the distance to focusing

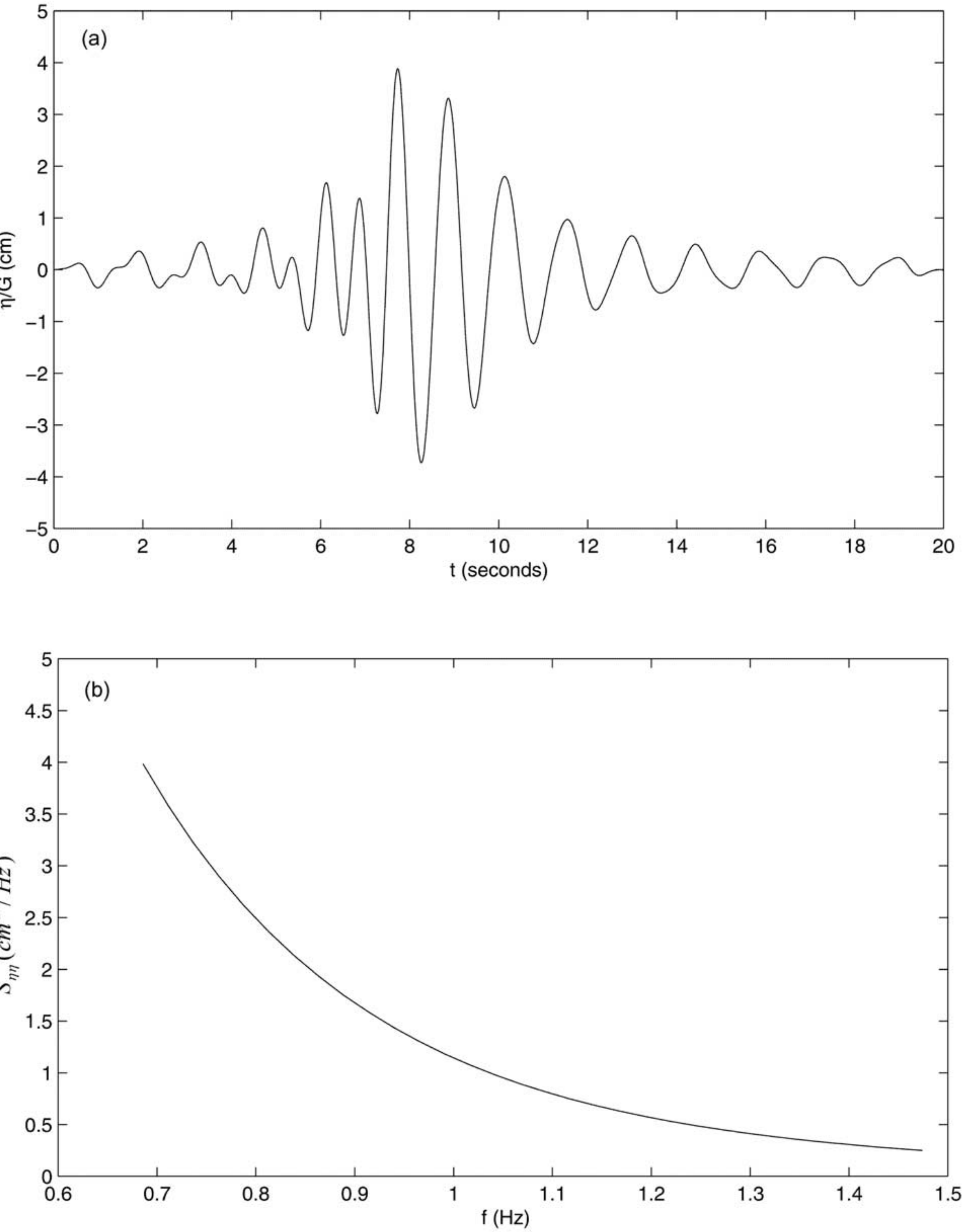

Figure 3. (a) Time series of input signals scaled by gain factor *G*. (b) Constant steepness spectrum.

location, x_f, yielding a dimensionless diffraction parameter, x_f/L_o. For a two-dimensional wave, L_o is infinite and x_f/L_o = 0 for all values of x_f, indicating that the two-dimensional breaking dynamics is insensitive to x_f, as demonstrated by *Rapp and Melville* [1990]. For three-dimensional waves, the effects of diffraction increase as x_f/L_o increases [*Nepf et al.*, 1998]. In this study, L_o was chosen to be 90 cm, i.e., three paddles long, resulting in a fixed x_f/L_o = 3.67.

[14] The full range of three-dimensional wave packet evolution in the basin can now be described by the non-dimensional set:

$$\eta k_c = \eta k_c \left[\theta_{\max} \text{ or } x_f/L_o,\ \Delta f/f_c, k_c d, a k_c\right], \quad (8)$$

where the central wave number, $k_c = 4.73\ \text{m}^{-1}$, corresponds to the central frequency, f_c, using equation (2). The maximum focusing angle $\theta_{\max}$ and diffracting parameter x_f/L_o were selected as described above. A single-frequency bandwidth ratio, $\Delta f/f_c = 0.73$, was selected because it produced the most distinct transition between the two-dimensional spilling and plunging cases as defined by *Rapp and Melville* [1990]. Moreover, the frequency bandwidth ratio was not varied in this study because *Rapp and Melville* [1990, Figure 17] showed that it has little influence on breaker onset and severity. For a short fetch and a broadband spectrum, as used in this study, nonlinear wave modulations are not pronounced in long-crested (two-dimensional) waves [*Baldock et al.*, 1996] and even less important for directional short-crested waves [*Stansberg*, 1992, 1995; *Johannessen and Swan*, 2001]. Therefore wave generation for the two-dimensional (equation (4)) and the three-dimensional (equations (6) and (7)) wave packets based on a linear wave theory can create desired wave groups in this study. The depth parameter $k_c d$ was chosen to produce deep water waves, eliminating the dependence of wave evolution on water depth. For a central wave number k_c, the value of $\tanh(k_c d) = 0.99$, indicating that the deep water wave condition was met at the scale of the wave packet.

[15] Finally, the intensity of breaking, from incipient to plunging waves, was varied through the gain, G, and parameterized by the global, spectrum-based wave steepness ak_c [*Rapp and Melville*, 1990], i.e.,

$$a k_c = \left(\sum_{n=1}^{32} a_n\right) k_c = G\left(\sum_{n=1}^{32} \frac{1}{k_n}\right) k_c, \quad (9)$$

where a_n is defined by equation (3). The classifications of an incipient wave (maximum nonbreaking wave), spiller, and plunger are defined following *Rapp and Melville* [1990]. Photographs depicting waves at each breaking condition were presented by *Rapp and Melville* [1990] (two-dimensional waves) and *Nepf et al.* [1998] (three-dimensional diffracting waves) and are not repeated here. Instead, images were chosen to demonstrate differences in crest geometry associated with directionality, specifically to compare plunging crests that are spatially focusing, diffracting, and two-dimensional (Figure 4). The two-dimensional wave is very uniform along the crest up to the point of breaking. Once the wave breaks, however, nonuniformity quickly sets in, as is observed in the Figure 4a. Between the short-crested waves, the spatially focusing plunger (Figure 4b) was more localized and energetic than the diffracting plunger (Figure 4c).

2.2. Breaking Wave Criteria

[16] Breaking wave criteria can be classified into three major categories. First, geometric criteria are based on the geometry of wave shape. Second, kinematic criteria are based on the characteristics of wave motions, e.g., particle velocity and wave phase speed. Third, dynamic criteria are based on the characteristics of wave energy. In the following sections (2.2, 2.3, and 2.4), we first discuss the methods for estimating the breaking criteria within each classification. Then, in section 3, we discuss the performance of each criterion.

2.2.1. Geometric Criterion

[17] Two types of wave shape parameter were considered here: (1) global wave steepness, ak_c, which characterizes the maximum potential steepness based on the sum of spectral components, and (2) local wave steepness and asymmetry. The latter includes the crest front steepness (ε), the crest rear steepness (δ) the vertical asymmetry factor (λ), and the horizontal asymmetry factor (μ), each of which is defined in Figure 5. These parameters are frequently used to characterize steep asymmetrical waves or breaking waves. Following *Kjeldsen and Myrhuag* [1979, 1980], these parameters were estimated from the temporal records of surface displacement using zero-downcross analysis and assuming that timescales and length scales are related by the dispersion relationship for deep water waves, i.e., $L = gT^2/2\pi$, where L and T are the wave length and wave period, respectively.

2.2.2. Kinematic Criterion

[18] The most common kinematic criterion is the ratio of particle velocity, $|\bar{U}|$, and phase speed C: with breaking predicted for $|\bar{U}|/C \geq 1$ [*Longuet-Higgins*, 1969; *Tulin and Li*, 1992]. To obtain the particle velocity and the phase speed from the measured surface displacements, we extended the Hilbert transform technique, previously applied to two-dimensional waves [*Melville*, 1983; *Hwang et al.*, 1989; *Huang et al.*, 1992], to directional wave fields as follows. Suppose that the surface fluctuations can be described as

$$Z(x,y,t) = \eta(x,y,t) + i\zeta(x,y,t), \quad (10)$$

where η $(x, y, t)$is the measured vertical surface displacement and ζ (x, y, t) is its conjugate part. The conjugate is related to m through the Hilbert transform as

$$\zeta(x,y,t) = -\frac{1}{\pi}\int_{-\infty}^{\infty} \frac{\eta(x,y,\tau)}{\tau - t} d\tau, \quad (11)$$

and can be interpreted as the horizontal surface displacement. If linear wave theory is assumed (see the detail discussion at the end of section 2.2.2), the local horizontal particle velocity can then be evaluated as

$$|\bar{U}| = \left[u(x,y,t)^2 + v(x,y,z)^2\right]^{1/2} = \frac{\partial\zeta}{\partial t}, \quad (12)$$

where $u(x, y, t)$ and $v(x, y, t)$ are the local velocity components along the longitudinal x and transverse y directions, respectively. The local phase speed, C, is defined as

$$C = \frac{2\pi f(x,y,t)}{|k(x,y,t)|}, \quad (13)$$

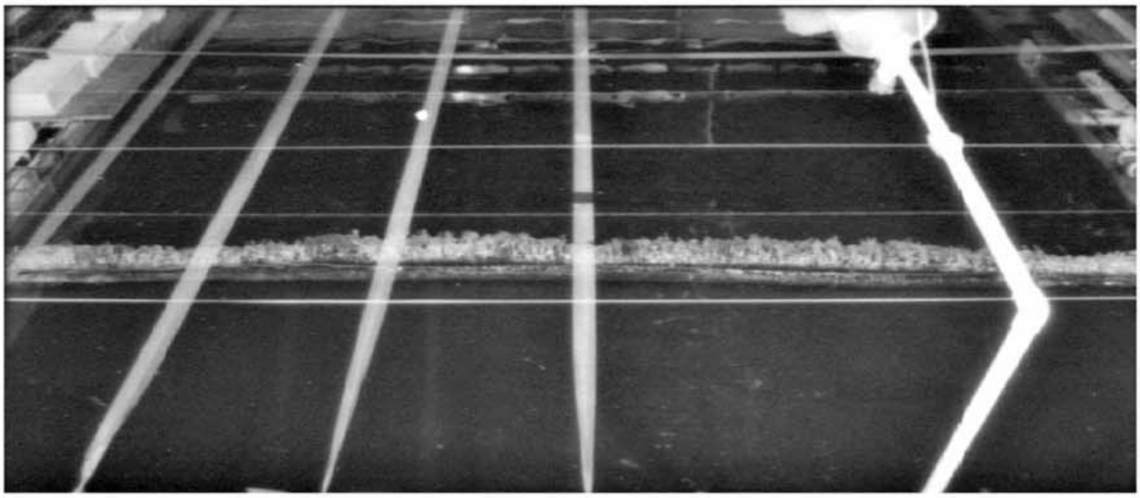

(a)

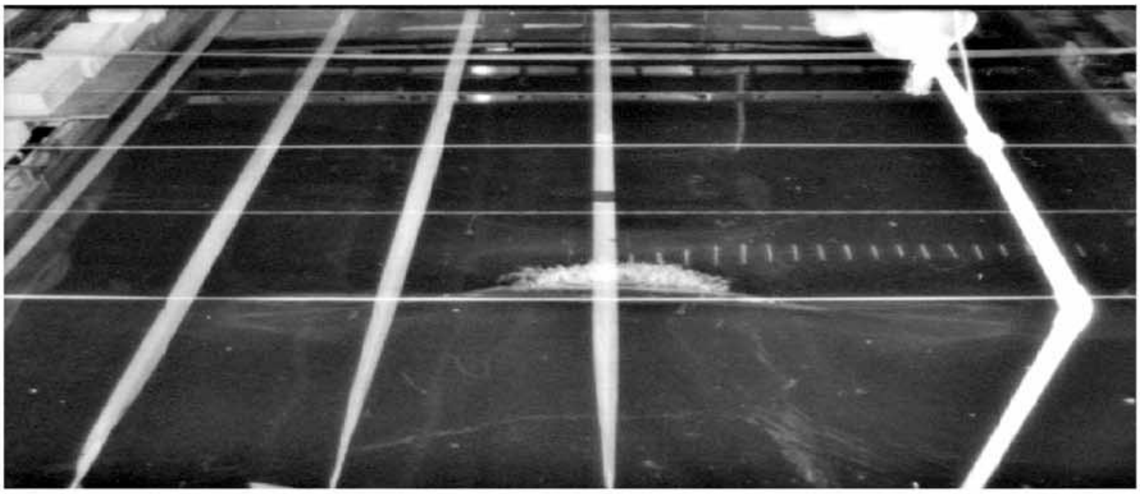

(b)

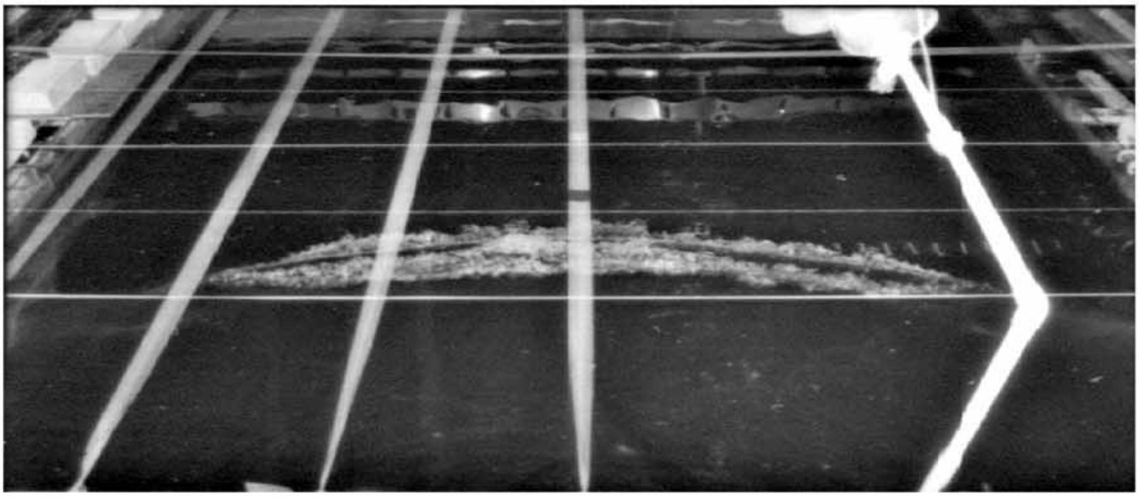

(c)

Figure 4. Photograph of plunging breaker taken at camera location 2 (backview): (a) two-dimensional plunger, (b) spatially focusing plunger, and (c) spatially diffracting plunger. Each lateral grid interval on the photograph corresponds to 50 cm.

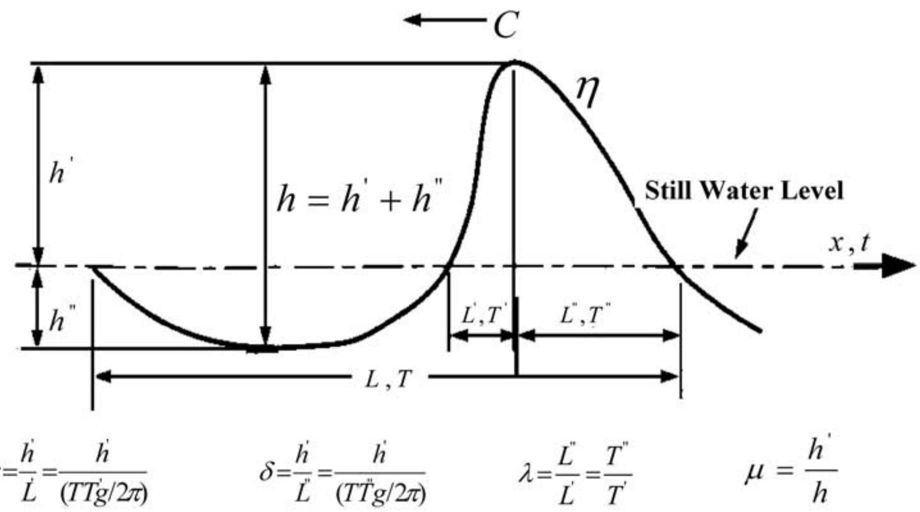

Figure 5. Definition of local wave parameters for steep asymmetric waves taken from *Kjeldsen and Myhuang* [1979]. The crest front steepness ε and the crest rear steepness δ were used to characterize wave height steepness. The vertical asymmetry factor λ and the horizontal asymmetry factor μ were used to characterize crest asymmetry. For each wave profile η, the prime and double primes for the *h* (wave height), *L* (wavelength), and *T* (wave period) are shown in Figure 5.

where $f(x, y, t)$ and $k(x, y, t)$ are the local frequency and the local wave number, which are estimated as follows. Note that equation (10) can be expressed in polar form as

$$Z(x, y, t) = A(x, y, t)e^{i\phi(x,y,t)}, \tag{14}$$

where $A(x, y, t) = [\eta(x, y, t)^2 + \zeta(x, y, t)^2]^{1/2}$ and $\phi(x, y, t) = \tan^{-1}[\zeta(x, y, t)/\eta(x, y, t)]$ are the instantaneous envelope and the local phase function, respectively. The local frequency is thus obtained by

$$f(x,y,t) = \frac{1}{2\pi}\frac{\partial\phi(x,y,t)}{\partial t} = \frac{\frac{\partial\varsigma}{\partial t}\eta - \frac{\partial\eta}{\partial t}\varsigma}{2\pi(\eta^2 + \varsigma^2)} \tag{15}$$

and the local wave number is evaluated by equation (2), i.e., $|k(x, y, t)| = 2\pi/gf^2(x, y, t)$ for the deep water condition. In this study, equations (12) and (13) were used to evaluate the parameter $|\vec{U}|/C$ for each time interval and spatial position. Threshold values of $|\vec{U}|/C$ were then correlated through comparisons to visual observations of breaking recorded on digital video images.

[19] It is important to reiterate that the definition of $|\vec{U}|$ given in equation (12) is based on a linear wave assumption and may underestimate the true crest velocity. *Baldock et al.* [1996] compared linear and second-order Stokes waves to the measured crest velocity of two-dimensional waves. They found that the measured crest velocity was 5∼30% larger than predicted by either theory, with the deviation decreasing with increasing wave spectrum bandwidth. For broadband spectrum, as used in this study, the predicted linear and second-order wave crest velocity was within 1 ∼ 5% of the measured wave crest velocity, depending on wave amplitude. In addition, recent three-dimensional wave measurements [*Johannesssen and Swan*, 2001] showed that increasing wave directionality can dramatically reduce the difference between linear/second-order Stokes wave and measured wave crest velocity. The above findings indicate that for a broadband spectrum, nonlinear wave modulations are not pronounced in two-dimensional waves and are even less important for directional short-crested waves [*Stansberg*, 1992, 1995]. This suggests that the linear wave assumption is a reasonable approximation for estimating wave crest velocity in a directional and broadband spectrum wave field, as used in this study.

[20] Similarly, the estimate of phase speed, given in equation (13) also uses a linear wave assumption that may lead to underestimation of the true phase speed. *Longuet-Higgins and Fox* [1977], *Kinsman* [1984], and *Jonsson and Steenberg* [1999] theoretically indicate that the limiting phase speed in a two-dimensional wave is approximately 10% larger than the linear wave phase speed. *She et al.* [1997] observed that the measured phase speed for a two-dimensional monochromatic wave is about 20% larger than that predicted by linear theory, consistent with the study of *Hedges and Kirkgoz* [1981]. However, a detailed laboratory study by *Baldock et al.* [1996] found only a 5% difference in phase speed between a linear and a second-order two-dimensional wave packet. This difference is even less for a three-dimensional focusing wave packet [*Johannesssen and Swan*, 2001]. These phase speed observations indicate that an increase in directionality and/or bandwidth can reduce the difference in phase speed between linear and nonlinear waves. From the above studies we conclude that the linear wave assumption can be a good approximation for phase speed with an error of 5∼20%. Finally, bringing the above discussion to bear, we estimate that the criterion, *U/C*, can be predicted for wave field considered in this study within 10% error.

2.2.3. Dynamic Criterion

[21] Wave focusing and subsequent breaking are manifested by an up frequency energy shift and subsequent energy loss, respectively [*Rapp and Melville*, 1990]. This signature suggests that the evolution of the higher harmonic

frequency band may be used as a dynamic criterion for breaking. The energy content of the higher harmonic frequency range was examined as follows. First, the surface displacement records were windowed for 40 s. Second, the spectrum, $S_{\eta\eta}$, associated with the windowed wave packet was calculated using an 8192 point FFT with a three-point moving-average filter. Third, the spectrum was divided into two frequency bands: the primary frequency band, 0.68~1.5 Hz, which corresponded to the input signal, and the higher-frequency band, above 1.5 Hz. The energy content of each frequency band, E_1 and E_2, respectively, was estimated by integrating the spectrum over the corresponding frequency range. The evolution of E_2 reflects the intrawave energy exchange associated with changes in wave steepness and asymmetry that occur as the wave focuses and approaches breaking. As with the kinematic parameter described above, visual observations of breaking were compared with the evolution of E_2.

2.3. Energy Losses

[22] Energy losses were estimated following a method developed for two-dimensional waves by *Rapp and Melville* [1990] and extended to short-crested waves by *Nepf et al.* [1998]. *Rapp and Melville* [1990] showed that, except near the point of breaking where the assumption of energy equipartition breaks down, the momentum and energy fluxes of a wave packet can be estimated from the surface displacement variance, $\overline{\eta^2}$, defined as

$$\overline{\eta^2} = \frac{1}{T_o}\int_0^{T_o} \eta^2 dt, \tag{16}$$

where the integration time, $T_o \approx N/\Delta f \approx 40$ s, can be calculated based on the modulation of wave components. The loss of wave energy within the test section is then given by the difference in the energy flux observed at the upstream and downstream ends. For the two-dimensional waves considered by *Rapp and Melville* [1990], this loss represents viscous dissipation in the wall and bottom boundary layers and the effects of wave breaking. When the waves are short-crested additional changes in local wave energy arise from diffraction and spatial focusing. However, these directional effects only reflect a lateral redistribution of wave energy and contribute no net loss to the laterally averaged packet. Thus the directional effects can be eliminated by applying a lateral average between the basin boundaries, i.e., between y = ±6*b*. Assuming that the group velocity is constant, the total loss of wave energy between an upstream (subscript '*o*') and downstream (subscript '*d*') position is the given by

$$D = \frac{\Delta \int_{-6b}^{6b} \overline{\eta^2} dy}{\left(\int_{-6b}^{6b} \overline{\eta_o^2} dy\right)} = \frac{\int_{-6b}^{6b} \overline{\eta_o^2} dy - \int_{-6b}^{6b} \overline{\eta_d^2} dy}{\left(\int_{-6b}^{6b} \overline{\eta_o^2} dy\right)}. \tag{17}$$

The lateral integration is evaluated using the wave gage records at the grid positions shown in Figure 1 and assumes symmetry across the centerline. The loss of wave energy, *D*, observed for the incipient (nonbreaking) condition is assumed to represent the viscous dissipation at the boundaries. Losses observed for the breaking wave packets that are in excess of those observed for the incipient case are then attributed to the breaking process. To properly compare the short-crested waves with the two-dimensional waves, the breaking loss is normalized by the observed breaking-crest length. Additional details of this technique are given by *Nepf et al.* [1998] and *Rapp and Melville* [1990].

3. Results

3.1. Surface Displacement Time Series

[23] Figure 6 compares the surface displacement record at the centerline of each wave-packet considered. For the incipient condition (Figure 6a), the two-dimensional and short-crested waves are quite similar. In each case dispersion was observed with the shorter waves leading before the theoretical focusing location, $x_f = 330$ cm, and trailing after, as prescribed by linear theory. Owing to nonlinearity, the actual location of wave breaking does not occur at the theoretical wave focus prescribed by the linear wave theory [*Rapp and Melville*, 1990; *Baldock et al.*, 1996]. For the spilling wave (Figure 6b), breaking was initiated on the leading crest at x = 370 cm (based on video observation) causing the wave height to decrease from x = 370 cm to 450 cm. The short-crested spilling waves began to deviate from the two-dimensional waves after x = 370 cm, reflecting that the differences in breaking intensity and that the effects of wave directionality had reached the centerline. The plunging breaker (Figure 6c) occurred one wavelength upstream at x = 270 cm. For the spatially focusing plunger, high frequency oscillations appeared in the surface displacement records after the breaking event, specifically at x = 290 cm and t = 10.5 s. These oscillations are attributed to the splashing and/or generation of random waves associated with the impact of the localized and highly energetic plunging jet against the water surface. These oscillations were absent from the two-dimensional and diffracting plungers because their jet structure was laterally more uniform and less energetic.

[24] The distinctive crest shape of each wave type is best observed by comparing the surface displacement records at different lateral positions (Figure 7). The two-dimensional wave packet produced a laterally uniform crest that broke simultaneously in space and time across the entire test section (Figure 7a, see also Figure 4). In contrast, both short-crested wave packets exhibited lateral variation in crest position and in breaking intensity (I, S, P), which was defined by visual observations. The diffracting wave crest was crescent-shaped with the centerline leading (Figure 7c). The breaking region of the focusing wave crest had a smaller lateral extent than the diffracting plunger, and a more synchronous peak arrival (Figure 7b). In addition, this crest cupped forward reflecting the focusing of wave energy toward a single point.

3.2. Geometric Breaking Criterion

3.2.1. Local Wave Shape Parameters

[25] The crest-front steepness, ε, measured along the crest at the onset of a plunging breaker is shown in Figure 8 for each of the wave types considered. While the two-dimen-

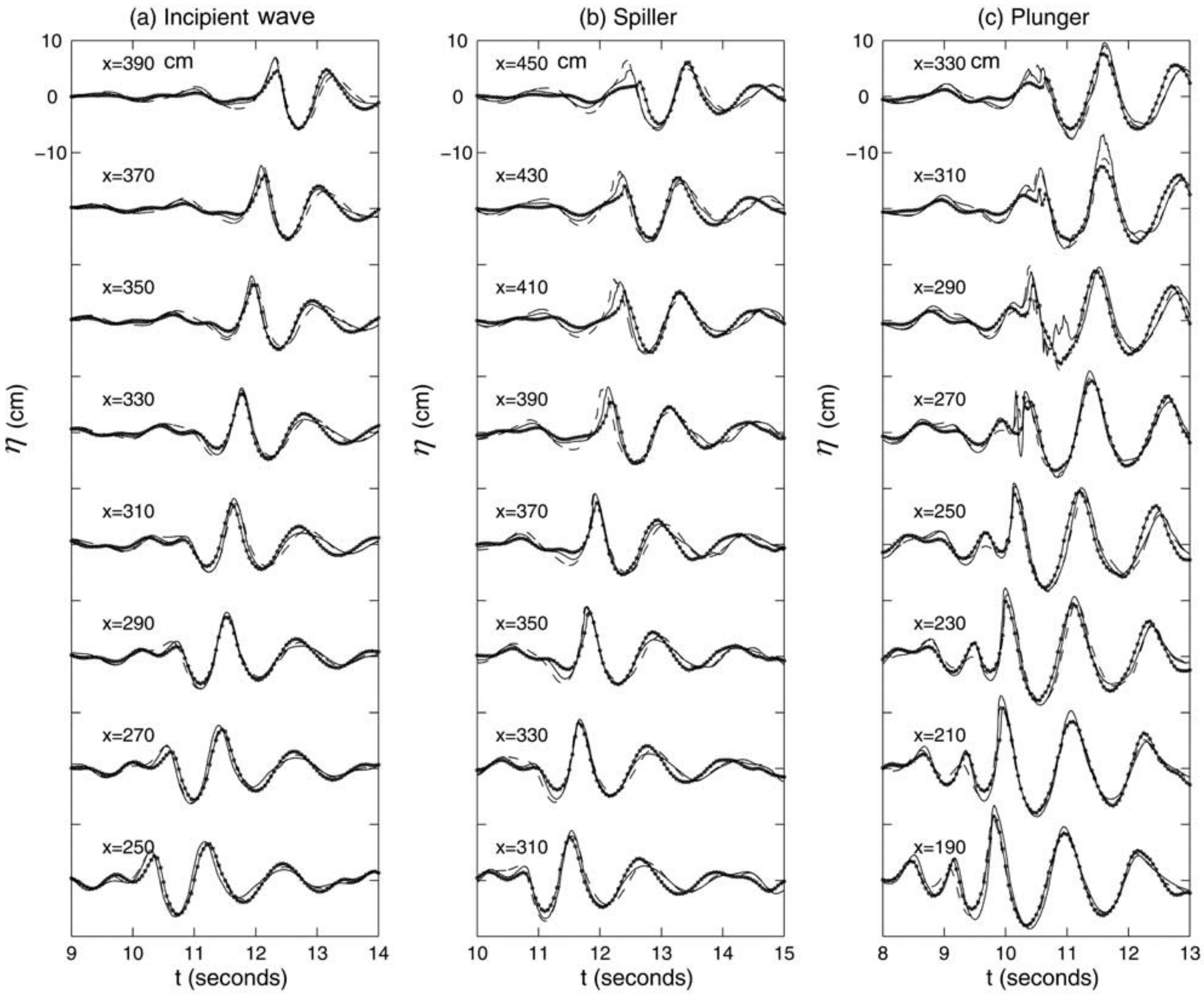

Figure 6. Surface displacement time series at the centerline, i.e., $y = 0$. The units for x and η are in centimeters away from the mean position of the paddles. The dashed lines, solid lines, and solid lines with dot correspond to two-dimensional, three-dimensional spatially focusing, and three-dimensional spatially diffracting waves, respectively: (a) incipient wave, (b) spiller, and (c) plunger.

sional crest exhibited a uniform steepness, $\varepsilon = 0.82$, the steepness of both directional crests decreased away from the centerline. Note that plunging was not precipitated for the focusing crest until the centerline steepness reached $\varepsilon = 1.22$. This is consistent with the previous spatial focusing experiments that observed an increase in both ε and breaking severity as the angle of wave interaction increased [*She et al.*, 1994; *Kolaini and Tulin*, 1995]. In contrast, the centerline criterion for the diffracting wave is comparable to the two-dimensional crest. For both directional waves, once plunging is precipitated at the centerline it occurs off-center at less than critical steepnesses. This suggests that the introduction of turbulence and/or surface instabilities by the centerline breaking provokes breaking off-center at less than the critical steepness, that is, reduces the effective breaking criteria. Similarly, *Ramberg and Griffin* [1987], *Kolaini and Tulin* [1995], and *Nepf et al.* [1998] observed lower breaking steepnesses in the presence of turbulence left by previous breaking events. These observations suggest that oceanic turbulence may lower breaking criteria in the field relative to values observed in pristine tanks or predicted by theory. The spilling condition also exhibited transcrest variation in ε, which was similar to that observed for the plunging criteria (Figure 8).

[26] Table 1 summarizes observations of ε, δ, λ, and μ from several laboratory and field experiments. First, note that for each of the two-dimensional wave conditions, breaking is initiated at comparable steepness. The crest front steepness is less than that of the Stokes limiting wave, confirming that unsteady waves are more sensitive to breaking [*Longuet-Higgins*, 1997]. Second, consistent with the previous results [*She et al.*, 1994; *Nepf et al.*, 1998], the present experiments show that the local wave shape parameters observed at the onset of breaking (left-hand columns) are strongly influenced by wave directionality. Specifically, the breaking wave steepness increased monotonically from a diffracting (negative focusing) wave through a planar wave (two-dimensional) to a spatially focusing wave. This sensitivity to wave directionality, along with transcrest variation in breaking steepness (Figure 8), may explain

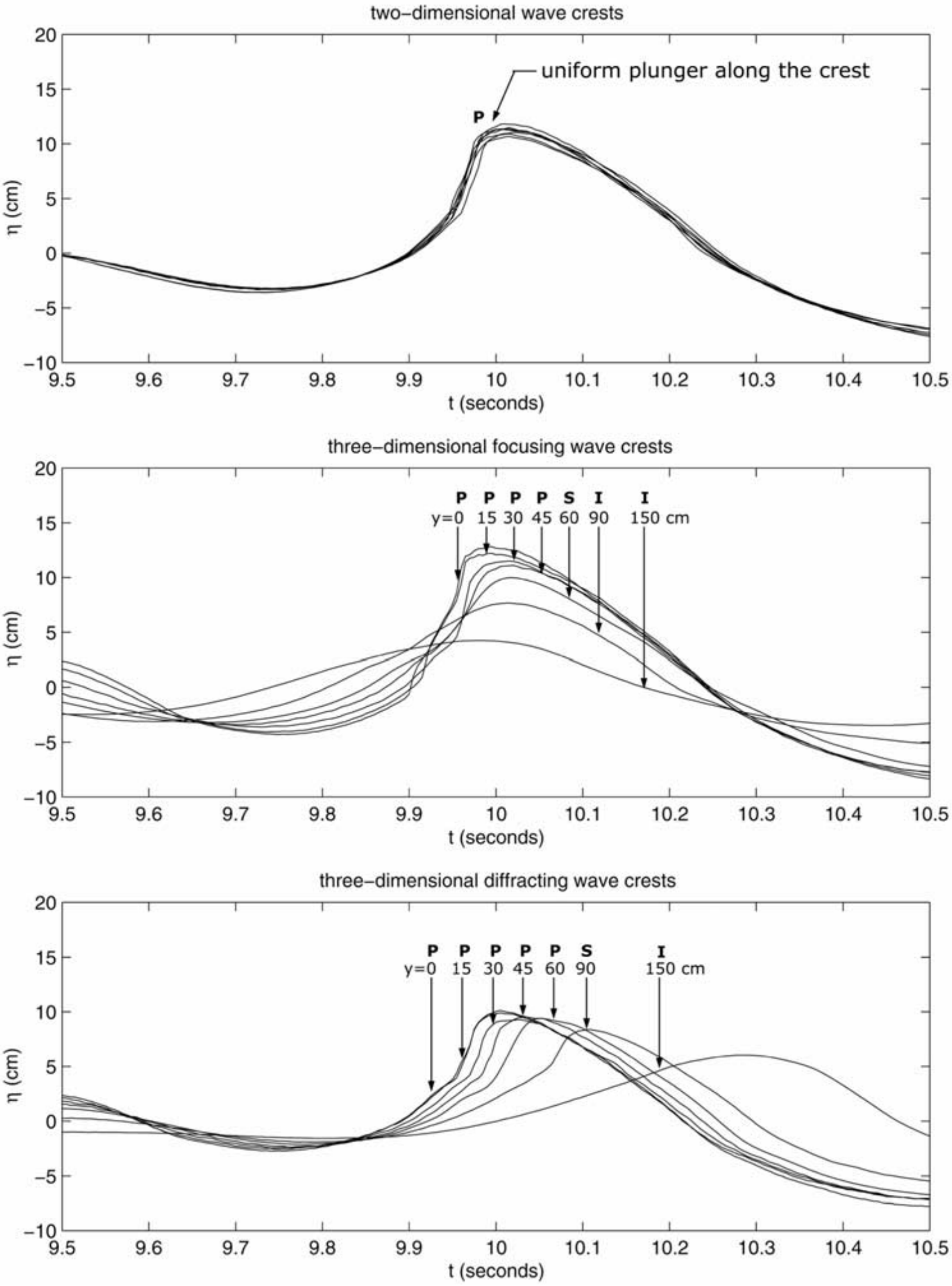

Figure 7. Comparison of surface displacement across the test section at x = 230 cm (the onset of plunging breaker). While wave crest of the two-dimensional plunger along the lateral locations were uniform, the wave crests of the three-dimensional focusing and diffracting waves along the lateral locations showed pronounced variation and consisted of a composite intensity of breaking, i.e., plunger (P), spiller (S), and incipient (I) wave, which are marked in Figure 7.

the range of local wave steepness observed in the field, e.g., $\varepsilon = 0.32 \sim 0.78$ [*Kjeldsen and Myrhaug*, 1979, 1980]. The crest rear steepness, δ, and vertical asymmetry factor, λ, have similar characteristics to those described for ε. Finally, consider the horizontal asymmetry, based on Stokes limiting waves, the onset of the spiller should occur at μ = 0.67. However, in this study, μ = 0.74 was observed for incipient waves without breaking, i.e., higher than that observed for spilling breakers. This suggests that μ is not sufficient to characterize the onset of breaking. To conclude, the compilation of several studies in Table 1 [*Kjeldsen and Myrhaug*, 1979, 1980; *Bonmarin*, 1989; *She et al.*, 1994] demonstrates the wide range of values observed for each criterion and suggests that local wave shape parameters are not robust indicators for oceanic wave breaking.

3.2.2. Spectrum-Based Global Wave Steepness

[27] Table 2 summarizes the spectrum-based global wave steepness, ak_c, under conditions of different spectral shape and wave directionality. Comparing the two-dimensional experiments [*Rapp and Melville*, 1990; *Lamarre*, 1993; *Chaplin*, 1996; *Kway et al.*, 1998] demonstrates the sensitivity of ak_c to variation in spectral shape. As a relatively

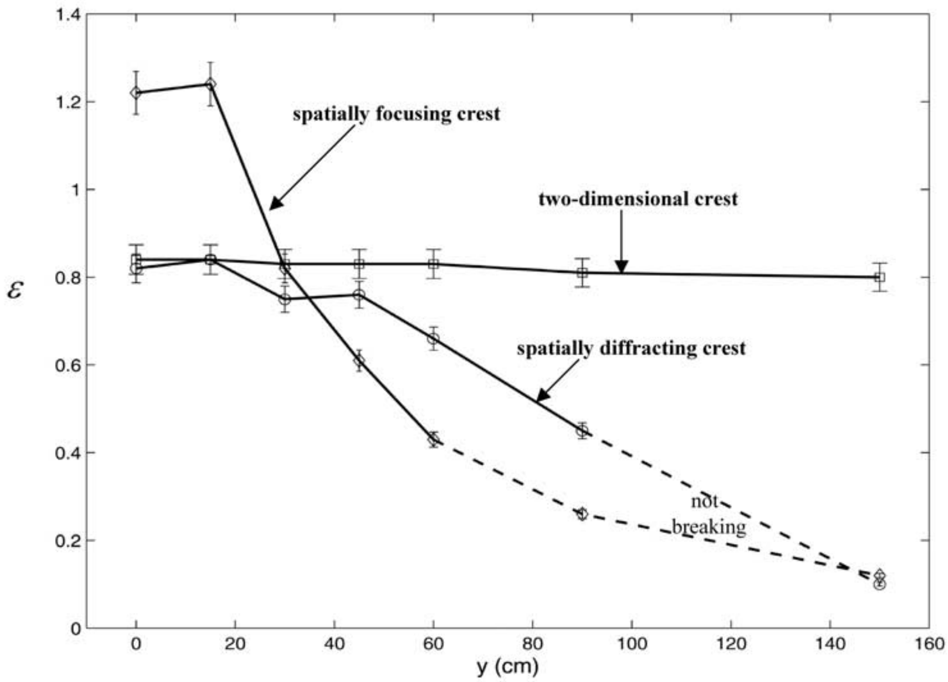

Figure 8. Crest front steepness at the onset of plunger. The solid (dashed) lines correspond to the regions where breaking does (does not) occur.

greater proportion of energy resides in the deep water-frequency components, from constant-amplitude through Pierson-Moskowitz to constant-steepness spectra, the global wave steepness, ak_c, is shifted upward. This suggests that wave fields consisting of relatively greater contributions of low-frequency energy are more stable with regard to this criterion, i.e., have higher thresholds for breaking. The new experiments presented here show that the global wave steepness is also sensitive to wave directionality. The incipient criteria decreased from the diffracting wave to the two-dimensional wave and then to the focusing wave (Table 2). The same trends are observed for the spilling and plunging criteria. Since both spectral shape and wave directionality affect the global wave steepness criteria, one should be cautious when extrapolating specific laboratory results to oceanic wave fields.

3.3. Kinematic Breaking Criterion

[28] When particle velocity $|\vec{U}|$ exceeds the phase speed C, breaking should occur [*Longuet-Higgins*, 1969]. On the basis of the two-dimensional, numerical wave tank simulations, *Wang et al.* [1993], *Yao et al.* [1994], and *Tulin* [1996] alternatively suggested that for deep water waves breaking is initiated when $|\vec{U}|$ exceeds the local wave group velocity, $C_g = 0.5C$, *i.e.* $|\vec{U}|/C = 0.5$. Two explanations can be offered for this discrepancy. First, the concept of group velocity is not well defined for nonlinear unsteady conditions such that the estimate of group velocity may

Table 1. Comparison of Geometry Breaking Criteria Based on Local Wave Shape Parameters

	ε		δ		λ		μ	
	Onset[a]	Breaker[b]	Onset[a]	Breaker[b]	Onset[a]	Breaker[b]	Onset[a]	Breaker[b]
Stokes limiting wave two-dimensional	0.48		0.48		1.00		0.67	
Kjeldsen and Myrhaug [1979, 1980] two-dimensional, field[c]	0.32	0.78	0.26	0.39	0.90	2.18	0.84	0.95
Bonmarin [1989] 2-D periodic or dispersive waves	0.31	0.85	0.26	0.33	0.72	3.09	0.60	0.93
She et al. [1994] 3-D focusing wave with a *Skyner* [1990] spectrum								
Single frequency	0.82	1.52	0.66	0.96	1.16	1.68	0.62	0.65
Multifrequency	0.51	1.02	0.30	0.68	1.10	2.25	0.65	0.67
Present experiments with a constant-steepness spectrum								
2-D	0.38	0.84	0.24	0.41	1.33	2.00	0.71	0.82
3-D diffracting	0.39	0.84	0.24	0.45	0.74	1.80	0.69	0.80
3-D focusing	0.41	1.26	0.27	0.52	1.34	2.60	0.70	0.86

[a] Parameter value at the onset of spilling.
[b] Parameter value for the largest plunger breaker observed.
[c] The parameters are calculated with reference to mean water level (MWL), different from still water level (SWL) in all the others.

Table 2. Comparison of Global Spectrum-Based Wave Steepness for Breaking

Breaking Type	Spectrum	*Rapp and Melville* [1990] 2-D	*Lamarre* [1993] 2-D	*Chaplin* [1996] 2-D	*Kway et al.* [1998] 2-D	Present Experiments 3-D Diffracting	2-D	3-D Focusing
Incipient wave	constant amplitude	0.25		0.265				
Incipient wave	constant steepness		0.35	0.30		0.36	0.32	0.21
Spiller	constant amplitude	0.30						
Spiller	constant steepness		0.40		0.59	0.43	0.40	0.26
Plunger	constant amplitude	0.39			0.25			
Plunger	constant steepness		0.45		0.73	0.66	0.50	0.47
Plunger	Pierson-Moskowitz[a]				0.38			

[a] Pierson-Moskowitz refers to the spectrum developed by *Pierson and Moskowitz* [1964].

vary significantly in deep water [*Longuet-Higgins*, 1997]. Second, the condition $|\vec{U}|/C = 0.5$ may differentiate a wave that will eventually evolve to breaking, but the actual breaking event doesn't occur until $|\vec{U}|/C = 1$ [*Wang et al.*, 1993]. Observations from the present experiments can be used to resolve the above issues. Using equations (12) and (13), the ratios of particle velocity $|\vec{U}|$, and wave phase speed, C, are calculated and shown as the solid lines in Figures 9, 10, and 11 for the incipient wave, spiller, and plunger, respectively. The dashed lines represent the threshold value of the proposed kinematic breaking criterion, $|\vec{U}|/C = 1$.

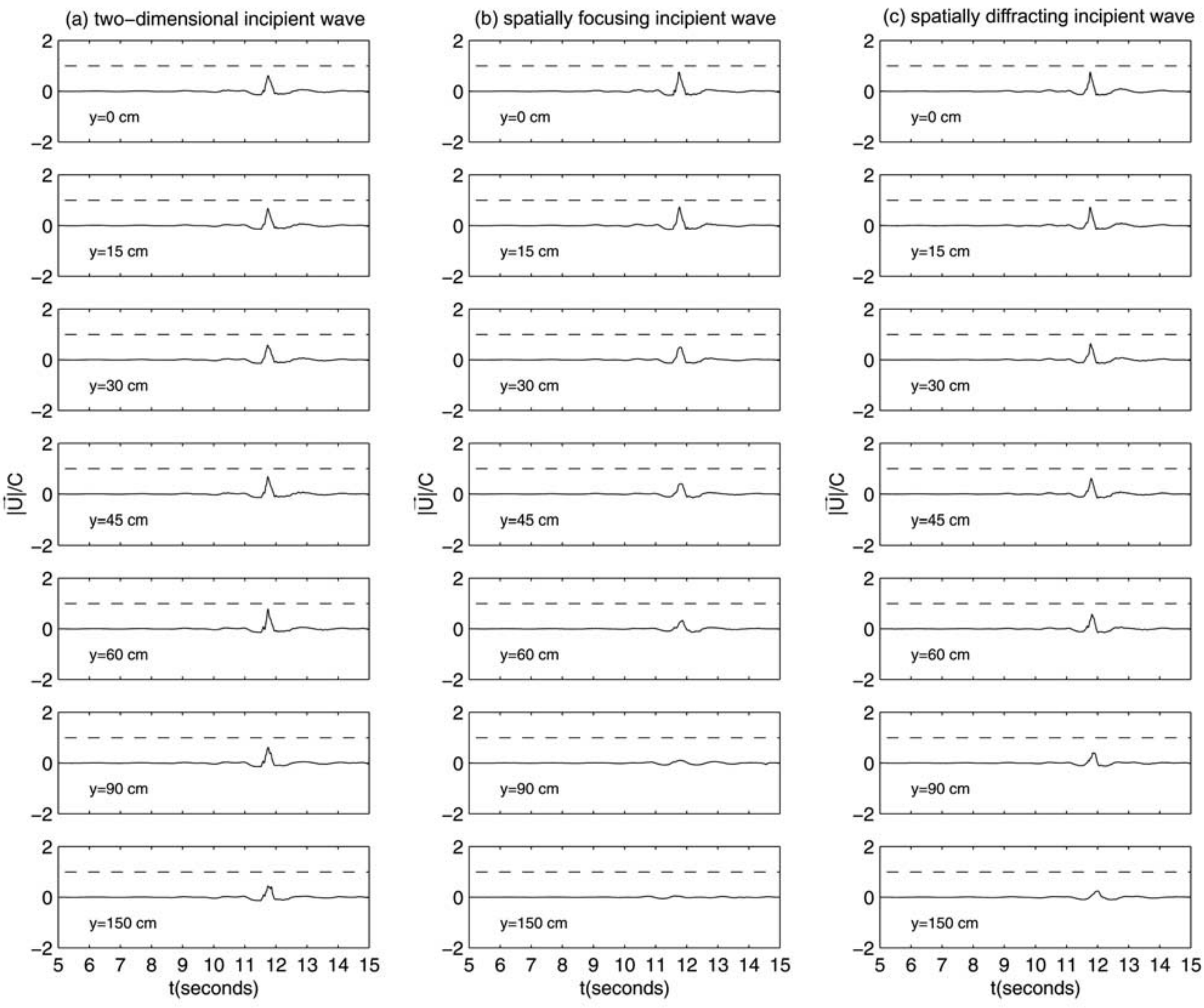

Figure 9. Ratio of particle velocity $|\vec{U}|$ and phase speed C at x = 330 cm for (a) two-dimensional incipient wave, (b) spatially focusing incipient wave, and (c) spatially diffracting incipient wave. The lateral position y is given in the bottom left of each graph. The dashed line is the threshold value of kinematic breaking criterion, where $|\vec{U}|/C = 1$. As shown in each graph, the ratio does not exceed the threshold value, indicating no breaking event.

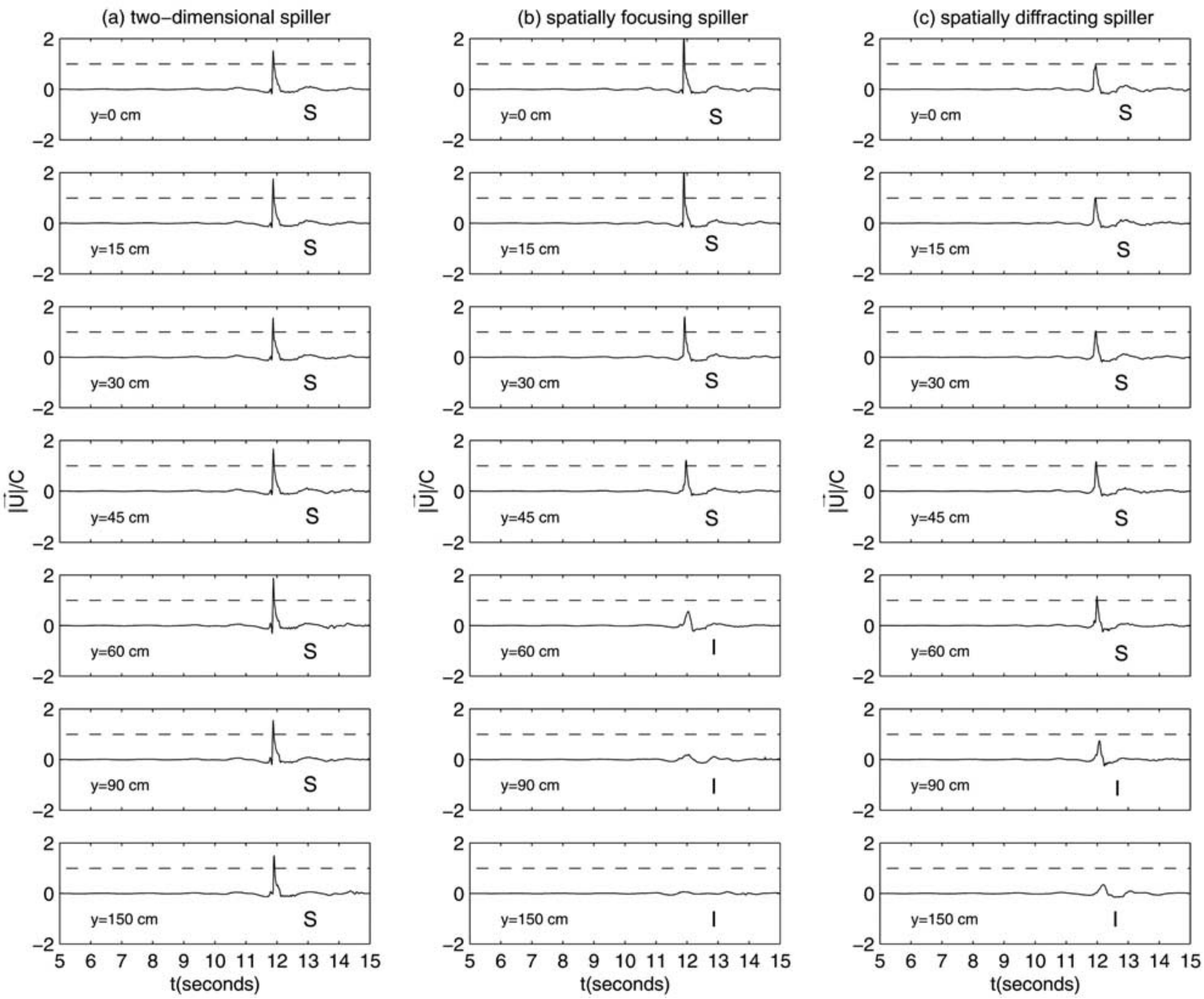

Figure 10. Ratio of particle velocity $|\vec{U}|$ and phase speed C at x = 370 cm for (a) two-dimensional spiller, (b) spatially focusing spiller, and (c) spatially diffracting spiller. The lateral position y is given in the bottom left of each graph. The dashed line is the threshold value of kinematic breaking criterion, where $|\vec{U}|/C = 1$. The letters, "S" and "I" in each graph correspond to the spiller and incipient wave, respectively, on video observations.

[29] For the incipient wave, we consider the longitudinal position x = 330 cm because it is the location at which the maximum particle velocity occurs. All three incipient waves (Figure 9) reach $|\vec{U}|/C > 0.5$ at some location along the wave crests but no breaking is initiated, suggesting that the criterion $|\vec{U}|/C = 0.5$ is not appropriate for detecting unsteady breaking waves. In addition, the ratio $|\vec{U}|/C$ remains less than one for all three incipient wave crests, consistent with the breaking criterion $|\vec{U}|/C \geq 1$.

[30] The criterion for a spilling breaker, as suggested by *Longuet-Higgins* [1969], is that the particle velocity must be slightly larger than the phase speed, i.e., $|\vec{U}|/C \geq 1$. For the two-dimensional spiller the ratio $|\vec{U}|/C$ exceeds one at all lateral positions at t = 12 s (Figure 10a). This is consistent with the video observation that showed spilling occurred uniformly and simultaneously across the test section at x = 370 cm and t = 12 s (i.e., see Figure 4a). For the spatially focusing spiller (Figure 10b), $|\vec{U}|/C \geq 1$ occurs at the lateral positions y = 0, 15, 30, and 45 cm but not at positions y = 60, 90, and 150 cm, consistent with video observations of breaking. Similarly, $|\vec{U}|/C \geq 1$ occurs along the crest of the diffracting spiller (Figure 10c) except at the lateral positions y = 90 and 150 cm, where, based on video observations, the crest was not breaking (i.e., see Figure 4c). The above examination shows that the condition $|\vec{U}|/C \geq 1$ estimated by using a linear wave assumption seems to be a good indicator for detecting spilling breakers.

[31] For a plunger to occur, the kinematic ratio should increase beyond that for the spiller. For example, using a Particle Image Velocimetry (PIV) technique, *Perlin et al.* [1996] and *Chang and Liu* [1998] showed that the particle velocity at the tip of a two-dimensional overturning jet reached 1.3 $\sim$ 1.6 times of the wave phase speed. *She et al.* [1997] observed $|\vec{U}|/C \approx 1$ for spatially focusing plungers, but they cautioned that their measurement of particle velocity at the crest may have suffered from reduced image quality. For the present experiments, the criterion $|\vec{U}|/C > 1.5$ consistently predicts the onset of plunging. For the two-dimen-

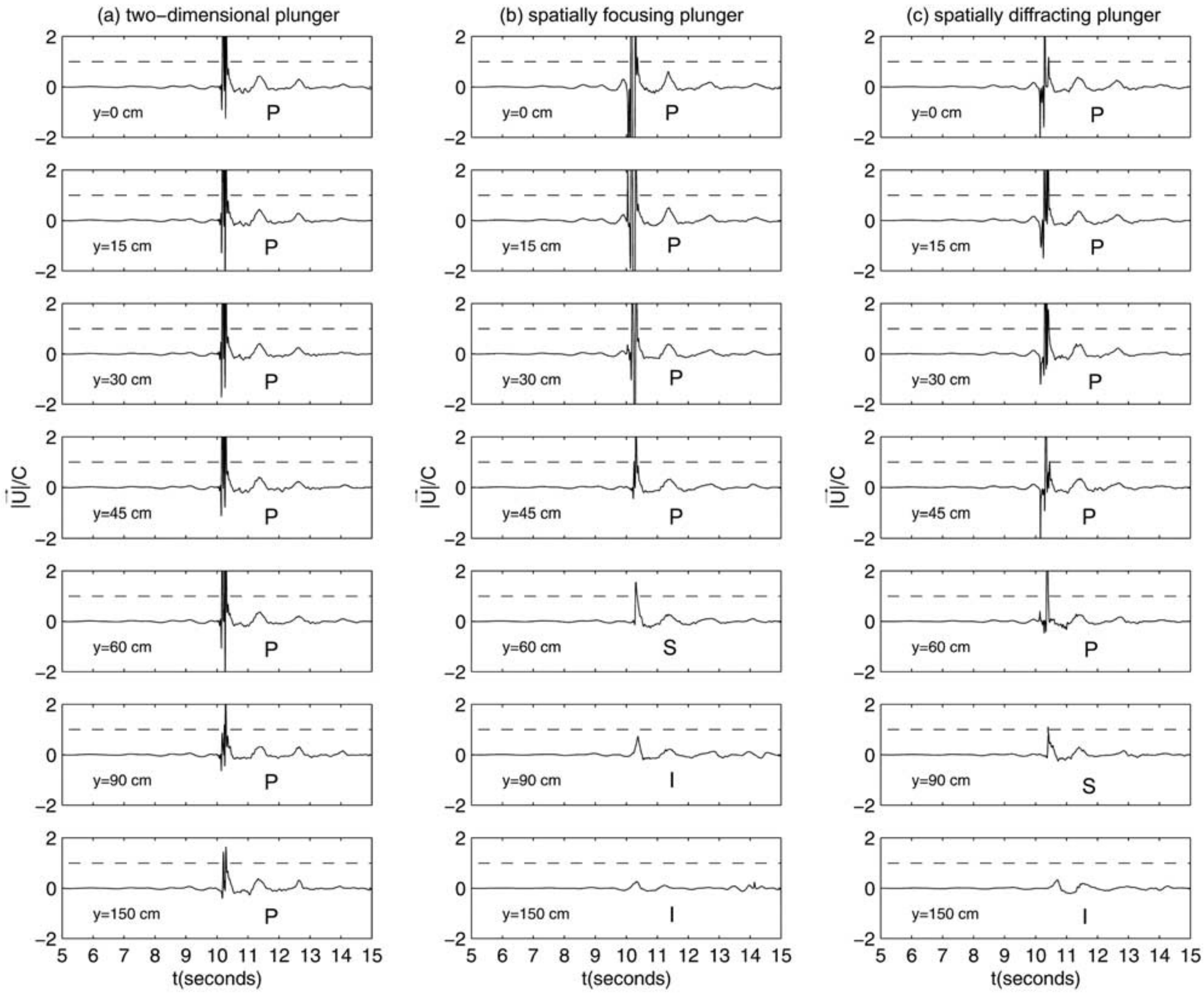

Figure 11. Same as Figure 10 but at x = 270 cm where (a) two-dimensional plunger, (b) spatially focusing plunger, and (c) spatially diffracting plunger occur. The letters, "P," "S," and "I" in each graph correspond to the plunger, spiller, and incipient wave, respectively, on video observations. Note that some ratios are below zero, which may result from the splashing.

sional plunger, video observation and wave gauge analysis indicate that plunging breaking is initiated at all lateral positions at t = 10.2 s (Figure 11a). For the spatially focusing (Figure 11b) and diffracting (Figure 11c) waves, $|\vec{U}|/C \geq 1.5$ is estimated at each lateral position for which plunging breaker occurs, and this threshold is not crossed where plunging breaker is not observed (e.g., Figure 4).

[32] The above observations demonstrate that the ratio $|\vec{U}|/C$ not only detects breaking but also reveals variation in breaking intensity along a wave crest, that is, the ratio robustly distinguishes plunger $\left(|\vec{U}|/C \geq 1.5\right)$, spiller $\left(|\vec{U}|/C \geq 1\right)$ and incipient wave $\left(|\vec{U}|/C < 1\right)$ along a single crest (Figures 11b and 11c). In addition, these observations indicate that this kinematic criterion is insensitive to wave directionality, as it works equally well for planar, diffracting, and focusing waves fronts, which is consistent with the observations by *She et al.* [1997].

[33] It might be surprising, particularly in a steep wave field, that a parameter evaluated with linear wave theory can be such a good indicator of breaking and thus, presumably, a good estimate of both $|\vec{U}|$ and C in a directional wave field with a broadband spectrum, as considered in this study. In contrast, for a two-dimensional monochromatic wave, the linear wave assumption may underestimate both $|\vec{U}|$ and C up to 20% [*She et al.*, 1997]. Since both are underestimated, their ratio, $|\vec{U}|/C$, can still be close to the actual ratio. As the purpose in this study is to suggest a robust method to detect wave breaking, and not to examine nonlinear effects on wave kinematics, we leave this issue for future study. We believe that, based on the observations presented here, the kinematic criterion evaluated using a Hilbert transform analysis and a linear wave theory is a promising and effective method for detecting oceanic breaking.

3.4. Dynamic Breaking Criterion

[34] The up frequency shift in wave energy associated with wave focusing has been observed for two-dimensional [*Rapp and Melville*, 1990; *Kway et al.*, 1998] and three-

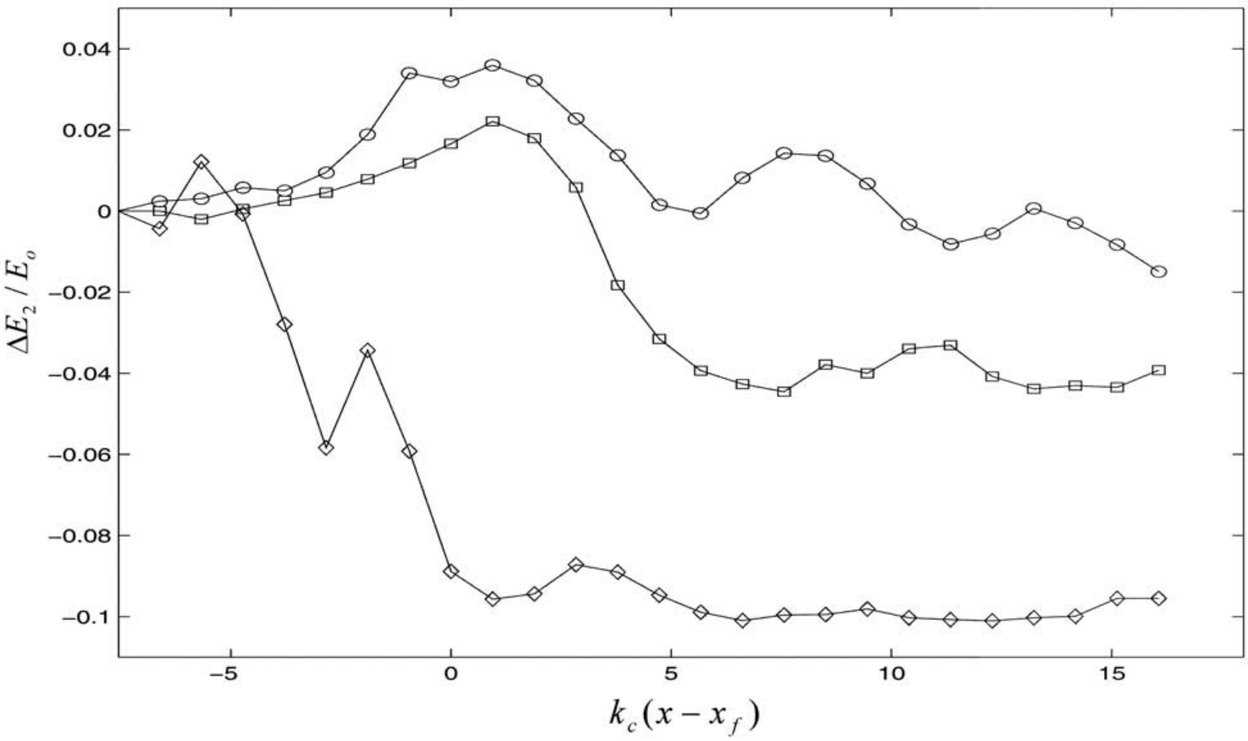

Figure 12. Evolution of E_2 for spatially focusing plunger (curve with diamonds), spiller (curve with squares), and incipient wave (curve with circles) at the centerline, i.e., $y = 0$ cm. Note that ΔE_2 is the difference of higher harmonic band energy with the reference at $x = 170$ cm. E_o is the total initial wave energy within each wave packet.

dimensional [*She et al.*, 1994; *Nepf et al.*, 1998] wave packets of different spectral shape. In the present experiments we investigated the effects of spatial focusing on this signature. For the incipient wave, the energy content of the higher harmonic band, E_2, (Figure 12) exhibited periodic behavior, increasing as the wave focuses and subsequently decreasing with little net change in energy downstream of the focal point. With breaking (both spiller and plunger), wave energy was shifted to the higher harmonic band and subsequently lost to the turbulent field. These results are consistent with similar observations made for two-dimensional and diffracting wave crests [*Nepf et al.*, 1998], indicating that wave directionality does not influence E_2 the signature. However, the observed evolution of E_2 is sensitive to the choice of reference position. In addition, multiple measurement positions are needed to construct the spatial evolution of E_2. For these reasons, the dynamic breaking criterion based on the evolution of E_2 is not as convenient or robust as the single-point kinematic criterion for detecting oceanic breaking.

3.5. Energy Losses

[35] Following the procedure described in section 2.3, the wave energy dissipation for the incipient wave, spiller, and plunger is calculated using (17). For each wave condition, i.e., the two-dimensional, focusing, and diffracting waves, the incipient wave-packet lost 10% of its energy. This loss is associated with viscous dissipation in the boundary layer and error in the lateral integration of wave energy. The additional energy loss observed for spilling and plunging wave packets, that is, beyond that observed for the incipient wave, is attributed to the breaking process. The breaking loss is normalized by the breaking crest length, which is (1.5 ± 0.3) m for the focusing plunger and is (2.2 ± 0.3) m

Table 3. Comparison of Energy Loss per Crest Length due to Breaking

Breaking Type	Spectrum	*Rapp and Melville* [1990] 2-D	*Lammare* [1993] 2-D	*Kway et al.* [1998] 2-D	Present Experiments[a]		
					3-D Diffracting	2-D	3-D Focusing
Plunger	constant amplitude	25		22			
Plunger	constant steepness		15	14	17 ± 2	16	32 ± 8
Plunger	Pierson-Moskowitz			20			
Spiller	constant amplitude	10		4			
Spiller	constant steepness		8		9 ± 1	10	12 ± 3

[a] The uncertainty of energy loss is due to the uncertainty of evolving breaking-crest length that is used to normalize the energy loss.

for the diffracting plunger. The same procedure is applied for the spilling breakers.

[36] Table 3 summarizes the energy loss per crest length due to breaking under conditions of different spectral distribution and wave directionality. First consider the two-dimensional crests. As suggested by *Kway et al.* [1998], the energy loss associated with plunging breaking increases as the spectral shape shifts toward the higher-frequency components (constant-amplitude, Pierson-Moskowitz, and constant-steepness spectra). The trend is similar, but less pronounced, for the spillers. This trend is consistent with the fact that most of the energy lost in the breaking process comes from the high frequency end of the spectrum [*Rapp and Melville*, 1990; *Lammare*, 1993]. New results from the present study demonstrated that wave directionality can also influence the fractional energy loss associated with wave breaking. With the same spectral shape (constant-steepness spectrum), the spatially focusing wave (32%) lost twice as much energy as the two-dimensional wave (16%). The energy loss for the diffracting wave, which was visibly milder than the focusing wave, was comparable to its two-dimensional counterpart. Since both wave directionality and spectral shape are shown to influence wave energy dissipation due to breaking, one should be cautious when extrapolating two-dimensional laboratory results to the spectrally evolving and directional wave fields in the open ocean.

4. Summary

[37] In this study, we generated fully three-dimensional breaking waves, i.e., spatially focusing and diffracting waves, by building on the two-dimensional, frequency-focusing technique for wave generation [*Rapp and Melville*, 1990]. The extended wave generation technique was used to examine the effects of wave directionality on breaking wave criteria and energy losses associated with wave breaking.

[38] The experimental results show that wave directionality, spectral shape and the introduction of turbulence by the antecedent breaking (e.g., at the centerline) can all affect the local wave shape parameters at the onset of breaking. These effects may explain the range of local wave shape criteria reported from field observations [*Kjeldsen and Myrhaug*, 1979, 1980] and explain why geometric local wave shape parameters have not proved to be stable limits for ocean wave breaking. A similar conclusion is reached with regard to the global steepness parameter, ak_c.

[39] Using single-point surface displacement measurements, a linear wave assumption and the Hilbert transform, *Hwang et al.* [1989] showed that the kinematic criterion $|\bar{U}|/C \geq 1$ is a good indicator for breaking for two-dimensional wind-generated waves. In this study, the above criterion is verified for a directional wave field using an aerial mapping of surface displacement measurements. Specifically, this study has shown that the ratio $|\bar{U}|/C$ not only detects breaking locations along a single crest but also reveals variation in breaking intensity. The ratio differentiates directional plunging and spilling with $|\bar{U}|/C \geq 1.5$ and $|\bar{U}|/C \geq 1$, respectively. Combining this promising result with previous studies for two-dimensional breaking [*Huang et al.*, 1992; *Griffin et al.*, 1996; *Seymour et al.*, 1998], we suggest that the single-point kinematic criterion evaluated using a Hilbert transform and linear wave theory can be a robust and effective indicator for wave breaking. This linear estimator has a critical value for breaking onset that is consistent with theory (U/C = 1), and with the observations of *Chang and Liu* [1998] and *Qiao and Duncan* [2001], who utilize nonlinear estimators. However, a recent article by *Stansell and MacFarlane* [2002], who also avoid linear approximations when estimating crest velocity and phase speed, observe breaking in two-dimensional waves at U/C less than one. In that study, breaking is consistently observed when $U/C > 0.72$. So, while all of the studies mentioned demonstrate that the kinematic ratio $U/C = 1$ segregates breaking and nonbreaking waves, the critical value for breaking onset is dependent on the estimator. Further investigations that examine the kinematic breaking criteria and formally extend the Hilbert transform method to nonlinear wave theory would be valuable to more precisely address the limitations of the linear technique and to allow a more direct comparison with other nonlinear estimators.

[40] The present experiments also show that spatial focusing and diffraction do not alter the up frequency transfer associated with wave steepening. However, this signature is not likely to prove useful in the field, because the evolution of E_2 is somewhat qualitative and very sensitive to the choice of reference location and because multiple-point measurements are required to interpret the evolution of E_2.

[41] Finally, the energy loss for the spatially focusing plunger is found to be about 2 times higher than that for the two-dimensional plunger, consistent with the suggestion that breaking severity increases with increasing spatial focusing angle [*She et al.*, 1994]. This observation suggests that wave directionality can play an important role in determining breaking losses. More measurements are required to resolve the relationship between energy loss and focusing angle across a wider parameter range.

[42] **Acknowledgments.** This research was supported by Office of Naval Research under contract N00014-94-1-0610. We would like to thank Paul Fricker for his assistance with taking the photographs and James B. Edson at Wood Holes Oceanographic Institution Wood Holes Institutions and Ole Madsen for their valuable discussions on breaking wave criteria. We specifically would like to thank the reviewers for providing valuable comments and suggestions on kinematic breaking criteria.

References

Baldock, T. E., C. Swan, and P. Taylor, A laboratory study of nonlinear surface waves on water, *Philos. Trans. R. Soc. London, Ser. A*, *452*, 649–676, 1996.

Banner, M. L., and D. H. Peregrine, Wave breaking in deep water, *Annu. Rev. Fluid Mech.*, *25*, 373–397, 1993.

Banner, M., and O. M. Phillips, On the incipient breaking of small scale waves, *J. Fluid Mech.*, *77*, 825–842, 1974.

Banner, M. L., and X. Tian, On the determination of the onset of breaking for modulating surface gravity water waves, *J. Fluid Mech.*, *367*, 107–137, 1998.

Benjamin, T., and J. Feir, The disintegration of wave trains in deep water, *J. Fluid Mech.*, *27*, 373–397, 1967.

Bonmarin, P., Geometric properties of deep water breaking waves, *J. Fluid Mech.*, *209*, 405–433, 1989.

Chang, K. A., and P. L. F. Liu, Velocity, acceleration and vorticity under a breaking wave, *Phys. Fluids*, *10*(1), 327–329, 1998.

Chaplin, J., On frequency-focusing unidirectional waves, *Int. J. Offshore Polar Eng.*, *6*, 131–137, 1996.

Cummins, W., The impulse response function and ship motion, *Schiffstech. Forschungsh. Schiffbau Schiffsmaschineubau*, *9*, 101–109, 1962.

Davis, M., and E. Zarnick, Testing ship models in transient waves, in *5th*

Symposium on Naval Hydrodynamics, *Rep. ACR-112*, pp. 509–540, Off. of Nav. Res., Arlington, Va., 1964.

Dean, R. G., and R. A. Dalrymple, *Water Wave Mechanics for Engineers and Scientists*, 353 pp., Prentice-Hall, Old Tappan, New Jersey, 1984.

Duncan, J. H., An experimental investigation of breaking waves produced by a towed hydrofoil, *Proc. R. Soc. London, Ser. A*, *377*, 331–348, 1981.

Duncan, J. H., The breaking and non-breaking wave resistance of a two-dimensional hydrofoil, *J. Fluid Mech.*, *126*, 507–520, 1983.

Easson, W. J., Breaking waves, *Offshore Tech. Rep. OTO-96-035*, U.K. Health and Safety Executive, London, 1997.

Greenhow, M., and T. Vinje, A theoretical and experimental study of the capsize of Salter's Duck in extreme waves, *J. Fluid Mech.*, *118*, 221–239, 1982.

Griffin, O. M., R. D. Peltzer, and H. T. Wong, Kinematic and dynamic evolution of deep water breaking waves, *J. Geophys. Res.*, *101*(C7), 16,515–16,531, 1996.

Hedges, T. S., and M. S. Kirkgoz, An experimental study of the transition zone of plunging breakers, *Coastal Eng.*, *4*, 319–333, 1981.

Huang, N. E., S. R. Long, C. C. Tung, M. A Donelan, Y. Yuan, and R. J. Lai, The local properties of ocean waves by phase-time method, *Geophys. Res. Lett.*, *19*(7), 685–699, 1992.

Hwang, P. A., D. Xu, and J. Wu, Breaking of wind-generated waves, measurements and characteristics, *J. Fluid Mech.*, *202*, 177–200, 1989.

Jessup, A. T., C. J. Zappa, and H. Yeh, Defining and quantifying microscale wave breaking with infrared imagery, *J. Geophys. Res.*, *102*(C10), 23,145–23,153, 1997.

Johannessen, T. B., and C. Swan, A laboratory study of focusing of transient and directionally spread surface water waves, *Philos. Trans. R. Soc. London, Ser. A*, *457*, 971–1006, 2001.

Jonsson, I. G., and C. M. Steenberg, Characteristic velocities for higher-order Stokes waves in deep water, *J. Waterw. Port Coastal Ocean Eng.*, *125*(3), 109–117, 1999.

Kerman, B. R., (Ed.), *Sea Surface Sound—Natural Mechanics of Surface Generated Noise in the Ocean*, 639 pp., Kluwer Acad., Norwell, Mass., 1988.

Kinsman, B., *Wind Waves, Their Generation and Propagation on the Ocean Surface*, 2nd ed., Dover, Mineola, N. Y., 1984.

Kjeldsen, S. P., and D. Myrhaug, Breaking waves in deep water and resulting wave forces, paper presented at 11th Offshore Technical Conference, Houston, Tex., 1979.

Kjeldsen, S. P., and D. Myrhaug, Wave-wave interactions, current-wave interactions and resulting extreme waves and breaking waves, paper presented at 17th Conference on Coastal Engineering, Am. Soc. of Civ. Eng., Sydney, N. S. W., Canada, 1980.

Kolaini, A., and M. P. Tulin, Laboratory measurements of breaking inception and post-breaking dynamics of steep short-crested waves, *Int. J. Offshore Polar Eng.*, *5*, 212–218, 1995.

Kway, J. H. L., Y. S. Loh, and E. S. Chan, Laboratory study of deep-water breaking waves, *Ocean Eng.*, *25*(8), 657–676, 1998.

Lamarre, E., An experimental study of air entrainment by breaking waves, Ph.D. thesis, Mass. Inst. of Technol., Cambridge, 1993.

Longuet-Higgins, M. S., On wave breaking and equilibrium spectrum of wind, *Proc. R. Soc. London, Ser. A*, *310*, 151–159, 1969.

Longuet-Higgins, M. S., Breaking waves in deep and shallow water, in *10th Conference in Naval Hydrodynamics*, *Publ. ACR-204*, pp. 597–605, Off. of Nav. Res., Arlington, Va., 1974.

Longuet-Higgins, M. S., Progress towards understanding how waves break, in *Proceedings of 21st Symposium on Naval Hydrodynamics*, pp. 7–28, Off. of Nav. Res., Arlington, Va., 1997.

Longuet-Higgins, M. S., and M. J. H. Fox, Theory of almost highest waves: The inner solution, *J. Fluid Mech.*, *80*, 721–741, 1977.

Longuet-Higgins, M. S., and R. W. Stewart, The changes in amplitude of short gravity waves on steady non-uniform current, *J. Fluid Mech.*, *10*, 529–549, 1961.

Loewen, M. R., and W. K. Melville, Microwave backscatter and acoustic radiation from breaking waves, *J. Fluid Mech.*, *224*, 601–623, 1991.

Melville, W. K., The instability and breaking of deep-water waves, *J. Fluid Mech.*, *115*, 163–185, 1982.

Melville, W. K., Wave modulation and breakdown, *J. Fluid Mech.*, *128*, 489–506, 1983.

Melville, W. K., Energy dissipation by breaking waves, *J. Phys. Oceanogr.*, *24*, 2041–2049, 1994.

Melville, W. K., Wave breaking in air-sea interaction, *Annu. Rev. Fluid Mech.*, *28*, 279–321, 1996.

Nepf, H. M., C. H. Wu, and E. S. Chan, A comparison of two- and three-dimensional wave breaking, *J. Phys. Oceanogr.*, *28*, 1496–1510, 1998.

Peregrine, D. H., Breaking waves on beaches, *Annu. Rev. Fluid Mech.*, *15*, 149–178, 1983.

Peregrine, D. H., Surf zone currents, *Theor. Comp. Fluid Dyn.*, *10*, 295–309, 1998.

Perlin, M., J. He, and L. P. Bernal, An experimental study of plunging breakers, *Phys. Fluids*, *8*(9), 2365–2374, 1996.

Phillips, O. M., The equilibrium range in spectrum of wind-generated wave, *J. Fluid Mech.*, *4*, 89–99, 1958.

Pierson, W. J., and L. Moskowitz, A proposed spectral form for fully developed wind seas based on similarity theory of S. A. Kitaigorodskii, *J. Geophys. Res.*, *69*, 747–757, 1964.

Qiao, H., and J. H. Duncan, Gentle spilling breakers: Crest flow-field evolution, *J. Fluid Mech.*, *439*, 57–85, 2001.

Ramberg, S. E., and O. M. Griffin, Laboratory study of steep and breaking deep water waves, *J. Water. Port Coastal Ocean Eng.*, *113*, 493–507, 1987.

Rapp, R. J., and W. K. Melville, Laboratory measurements of deep water breaking waves, *Philos. Trans. R. Soc. London, Ser. A*, *331*, 735–780, 1990.

Rosengaus-Moshinsky, M., Experimental study of wave generated bedforms and resulting wave attentuation, Ph.D. thesis, Mass. Inst. of Technol., Cambridge, 1987.

Seymour, R., C. A. Zimmermann, and J. Zhang, Discriminating breaking in deep water waves, in *Ocean Wave Kinematics, Dynamics and Loads on Structures*, edited by J. Zhang, pp. 305–313, Am. Soc. of Civ. Eng., Reston, Va., 1998.

She, K., C. A. Greated, and W. J. Easson, Experimental study of three-dimensional wave breaking, *J. Waterw. Port Coastal Ocean Eng.*, *120*(1), 20–36, 1994.

She, K., C. A. Greated, and W. J. Easson, Experimental study of three-dimensional breaking waves kinematics, *Appl. Ocean Res.*, *19*, 324–329, 1997.

Stansberg, C. T., On spectral instabilities and development of non-linearities in deep-water propagation wave trains, paper presented at 23rd International Conference on Coastal Engineering, Am. Soc. of Civ. Eng., Venice, Italy, 1992.

Stansberg, C. T., Effects from directionality and spectral bandwidth on non-linear spatial modulation of deep water surface gravity wave trains, paper presented at 24th International Conference on Coastal Engineering, Am. Soc. of Civ. Eng., Kobe, Japan, 1995.

Stansell, P., and C. MacFarlane, Experimental investigation of wave breaking criteria based on wave phase speeds, *J. Phys. Oceanogr.*, *32*(5), 1269–1283, 2002.

Su, M. Y., Three-dimensional deep-water waves, Part 1, Experimental measurements of skew and symmetric wave pattern, *J. Fluid Mech.*, *124*, 73–108, 1982.

Su, M. Y., M. Bergin, P. Marler, and R. Myrick, Experiment on nonlinear instabilities and evolution of steep gravity-wave trains, *J. Fluid Mech.*, *124*, 45–72, 1982.

Thorpe, S. A., Energy loss by breaking waves, *J. Phys. Oceanogr.*, *23*, 2498–2502, 1993.

Thorpe, S. A., Dynamical process of transfer at the sea surface, *Prog. Oceanogr.*, *35*, 315–352, 1995.

Tulin, M. P., and J. Li, On the breaking of energetic waves, *Int. J. Offshore Polar Eng.*, *2*, 46–53, 1992.

Wang, P., Y. Yao, and M. P. Tulin, Wave groups, wave-wave interaction and wave breaking, result of numerical experiments, paper presented at 3rd International Offshore and Polar Engineering Conference, Int. Soc. of Offshore and Polar Eng., Singapore, 1993.

Yao, Y., P. Wang, and M. P. Tulin, Wave groups, wave-wave interaction and wave breaking, result of numerical experiments, in *Proceedings of the 20th Symposium on Naval Hydrodynamics*, pp. 551–567, Natl. Acad. Press, Washington, D. C., 1994.

C. H. Wu, Department of Civil and Environmental Engineering, University of Wisconsin-Madison, Madison, Wisconsin, USA.

H. M. Nepf, Parsons Laboratory, Department of Civil and Environmental Engineering, Massachusetts Institute of Technology, Cambridge, Massachusetts, USA.